a

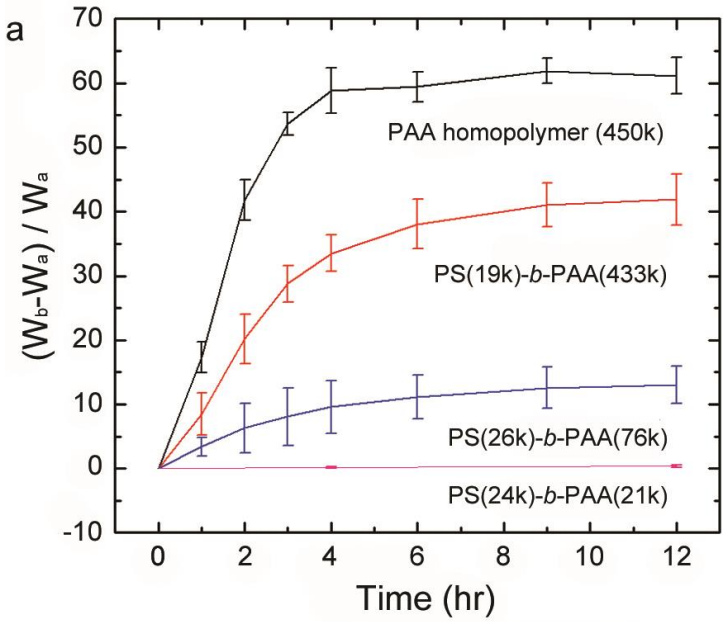

b

Samples (weight fraction of PS, wt_{PS})	Compressive modulus (MPa)
PAA homopolymer	0.02 ± 0.01
PS(19k)-*b*-PAA(433k) (wt_{PS}: 0.04)	0.08 ± 0.01
PS(26k)-*b*-PAA(76k) (wt_{PS}: 0.25)	0.23 ± 0.05
PS(24k)-*b*-PAA(21k) (wt_{PS}: 0.53)	107.20 ± 35.50
Fresh porcine skin	0.62 ± 0.18
Fresh porcine intestine	0.09 ± 0.02

Supplementary Figure S1. Swelling and mechanical properties as a function of the PS-*b*-PAA block copolymer composition. a, Swelling kinetics of PAA homopolymer and PS-*b*-PAAs (4 mm disc with 1 mm thickness) in PBS buffer (pH 7.4) at room temperature. W_a indicates the initial weight of samples at dry state and W_b is the weight of swollen samples. b, Compressive modulus obtained for the polymers at maximum swollen state and for skin and intestine tissues (tests were performed from the low strain range (0-5%)). Error bars represent standard deviation (n=5).

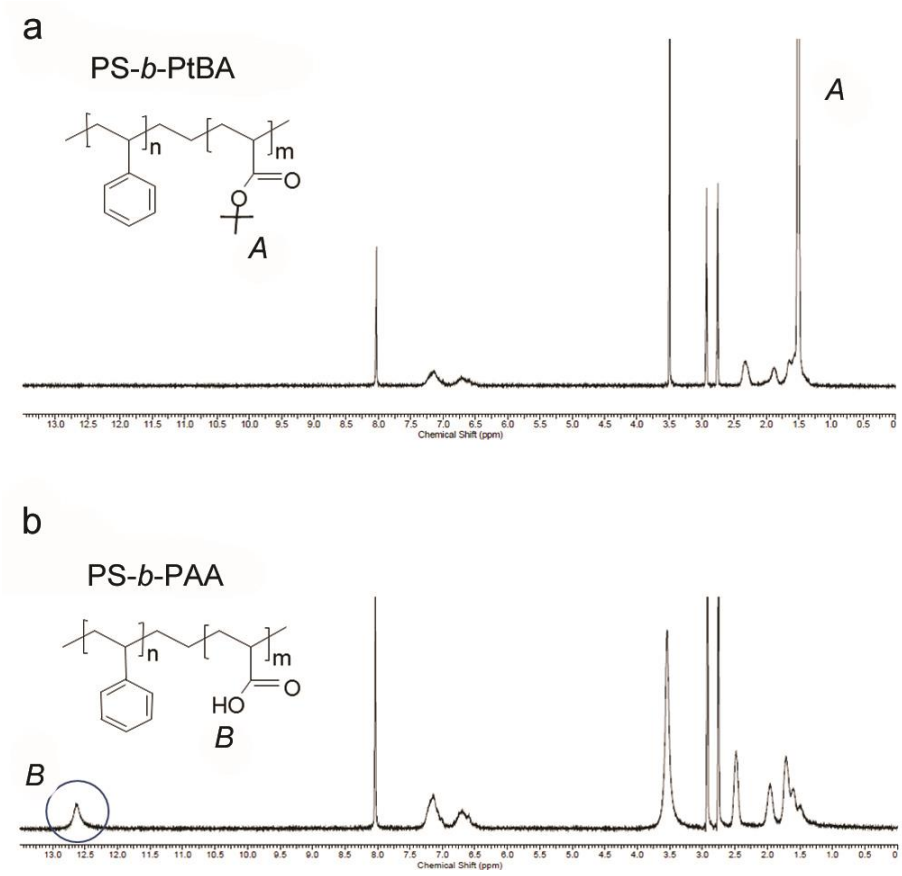

Supplementary Figure S2. ^{1}H NMR (DMF-d_7) spectra of a, PS-*b*-PtBA and b, PS-*b*-PAA. Peak at 1.45 ppm in Supplementary Figure S2a corresponds to methyl ester protons of *t*BA that disappeared after the reaction and the hydroxyl peak from the carboxylic acid (12.6 ppm) appeared (Supplementary Figure S2b). This result indicated that the *t*BA was fully converted to acrylic acid.

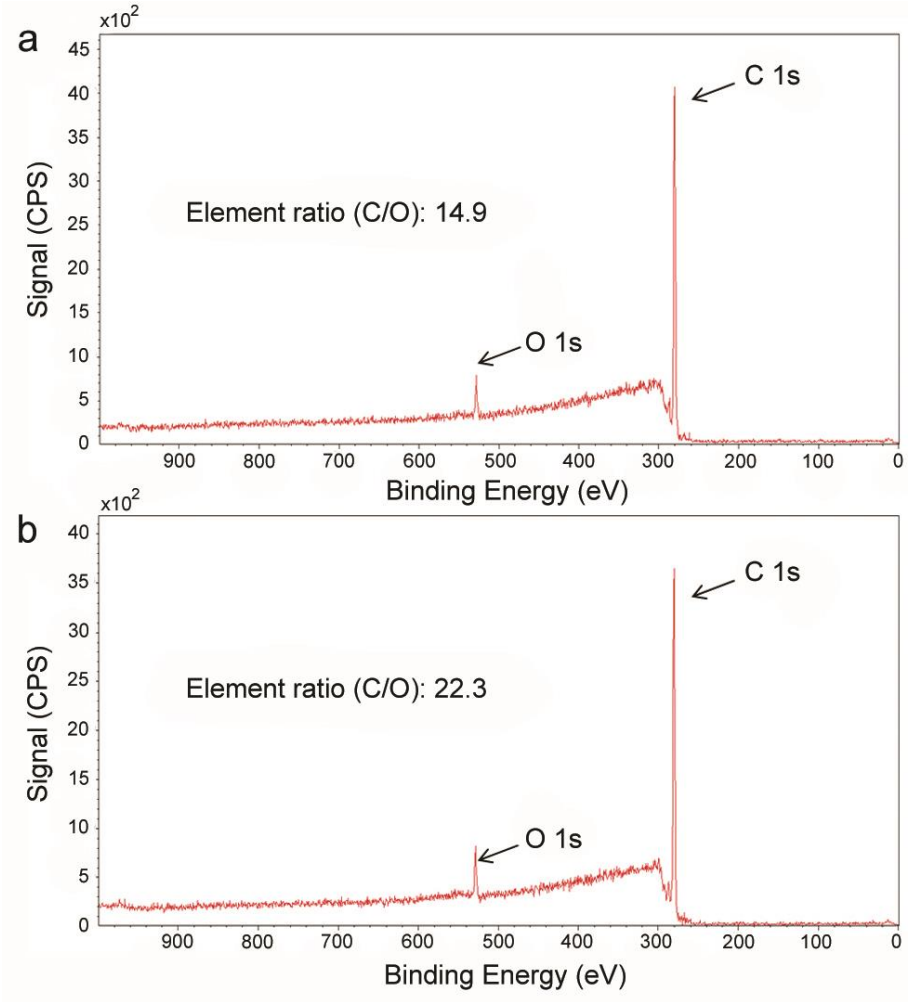

Supplementary Figure S3. XPS spectra obtained from the surface of PS-*b*-PAA films fabricated on a, a PDMS substrate and b, on a PS brush grafted on the Si wafer. PS-*b*-PAA films prepared on a PDMS or PS surface exhibited high C/O ratios that likely are from the PS block and not from the PAA block (theoretical C/O ratio for PAA is 1.5). The XPS data suggests that a thin PS layer was selectively located both on the outer-most surface of the MN and at interface between the swellable tip and PS core in the double-layered microneedle.

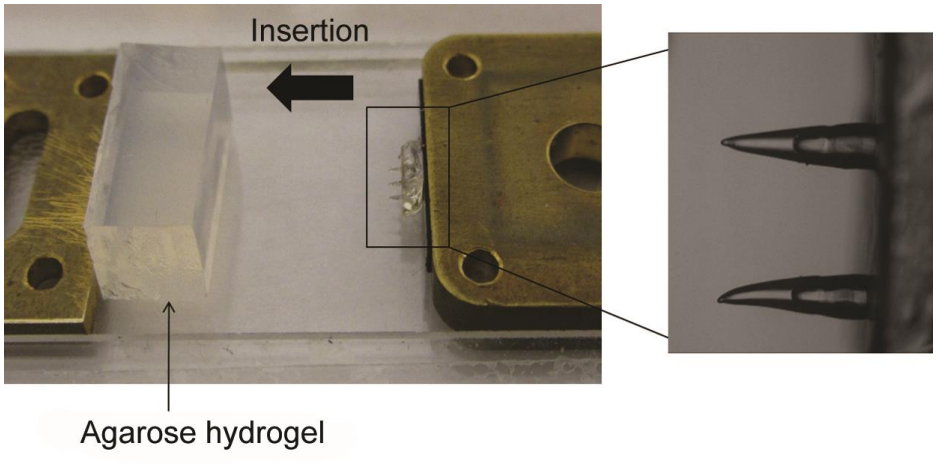

Supplementary Figure S4. Experimental set-up for *in-situ* measurements of BCP MN swelling within an agarose hydrogel. Swellable BCP MNs attached to a metal specimen with double-side tape was brought into contact with the hydrogel (supported by a fixed metal plate and an overhanging plastic substrate). Due to transparency of hydrogel, the swelling behavior of the MN was easily observed with an inverted microscope.

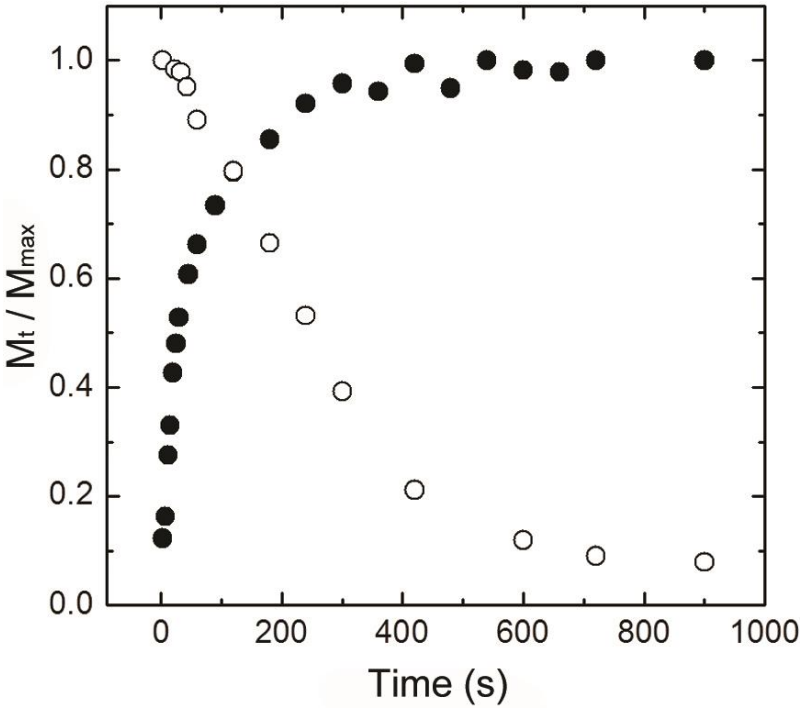

Supplementary Figure S5. Swelling kinetics (closed circle) after placement of the BCP MN into 1.4 wt% agarose hydrogels and deswelling (open circle) following removal measured by the change in volume of the swellable layer. M_t is the absorbed amount of water at time (t) and M_{max} is the absorbed amount of water at maximum swollen state.

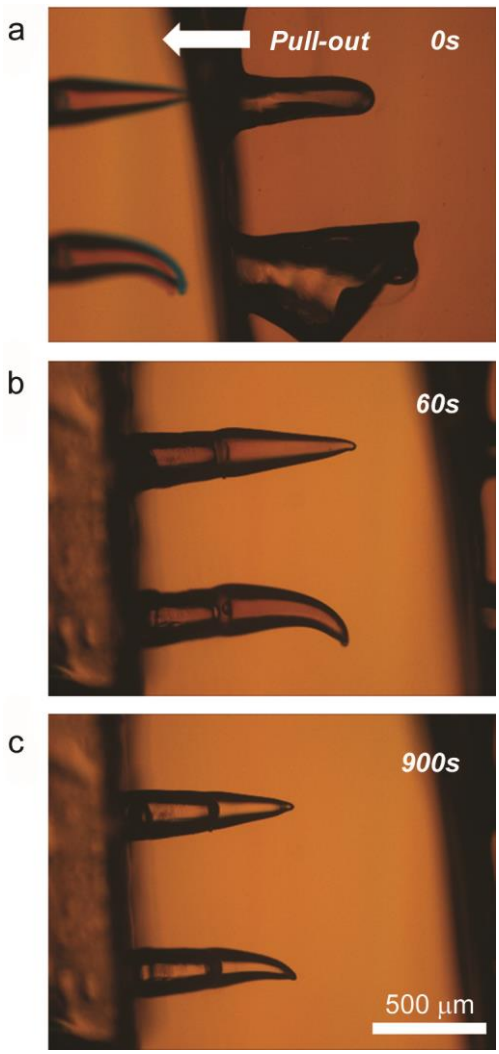

Supplementary Figure S6. BCP MN quickly return to their original state following removal from a hydrogel. Images acquired a, immediately following removal, and after b, 60s, and c, 900s at ambient conditions. The original conical structure of BCP MN was recovered after drying for 10-15 mins.

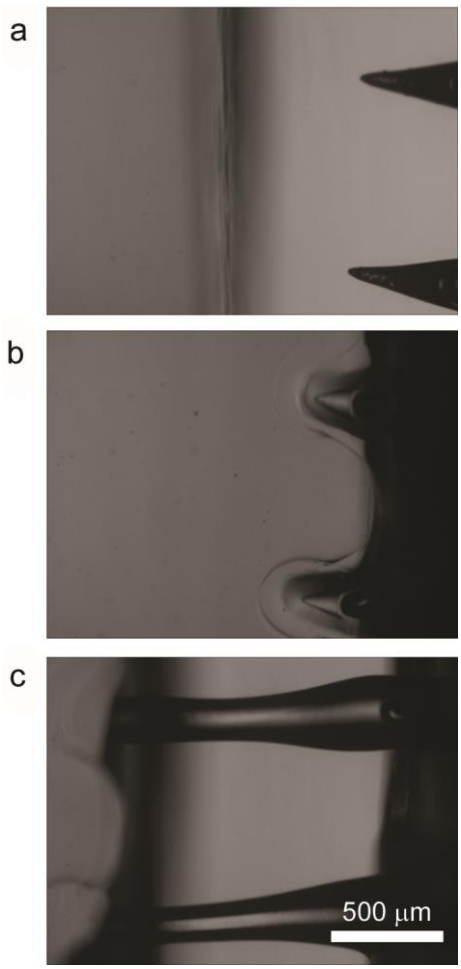

Supplementary Figure S7. a-c, Insertion test into 1.4wt% agarose gel for MNs prepared from pure poly acrylic acid (PAA, Mw:450k, sigma). PAA MNs were fabricated by solvent casting of 20 wt% PAA solution dissolved in DMF with a PDMS mold for 48 hr. After drying at 180^{o}C for 4hr, insertion tests were performed. a, Conical PAA MN b, did not penetrate into the hydrogel due to a low mechanical strength of swollen PAA and c, swollen PAA MNs detached from the hydrogel.

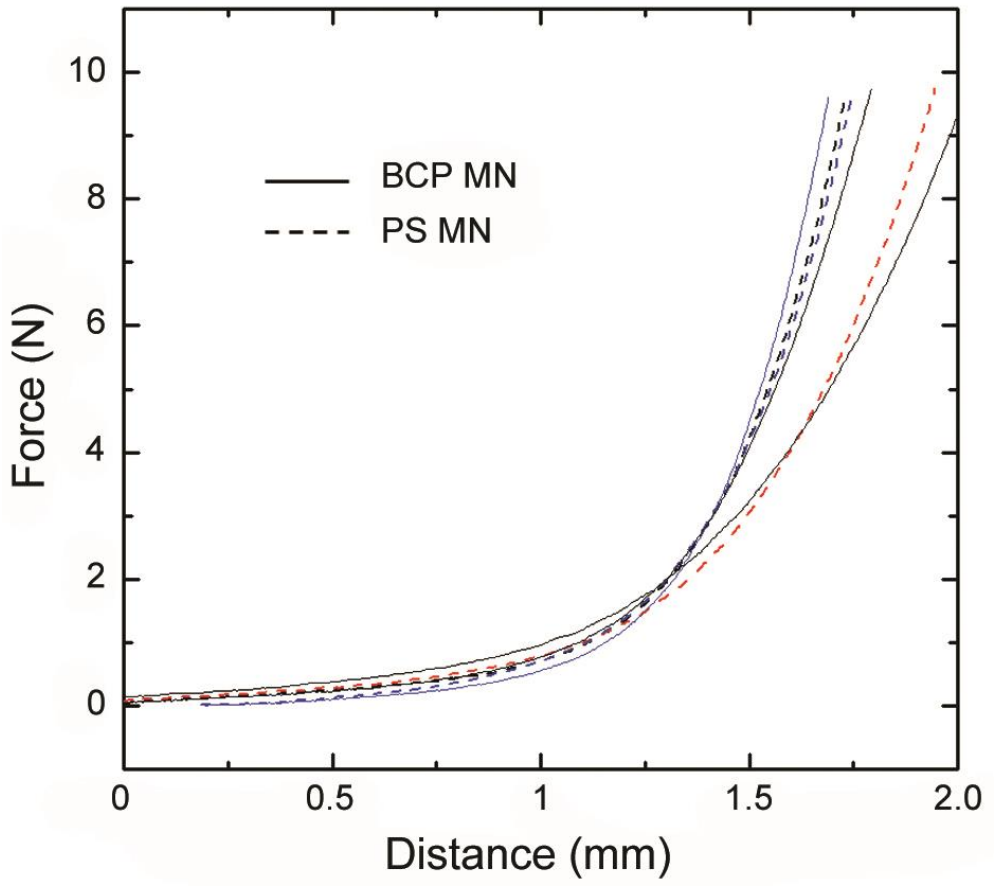

Supplementary Figure S8. Force versus displacement plots obtained by insertion of 10 x 10 MN in 1 cm^2 arrays of BCP MNs (with a swellable tip height of 40%) and PS MNs into pig skin at an insertion velocity of 100 mm/min. Swellable BCP MNs and non-swellable PS MNs showed similar force versus displacement profiles during insertion (n=3).

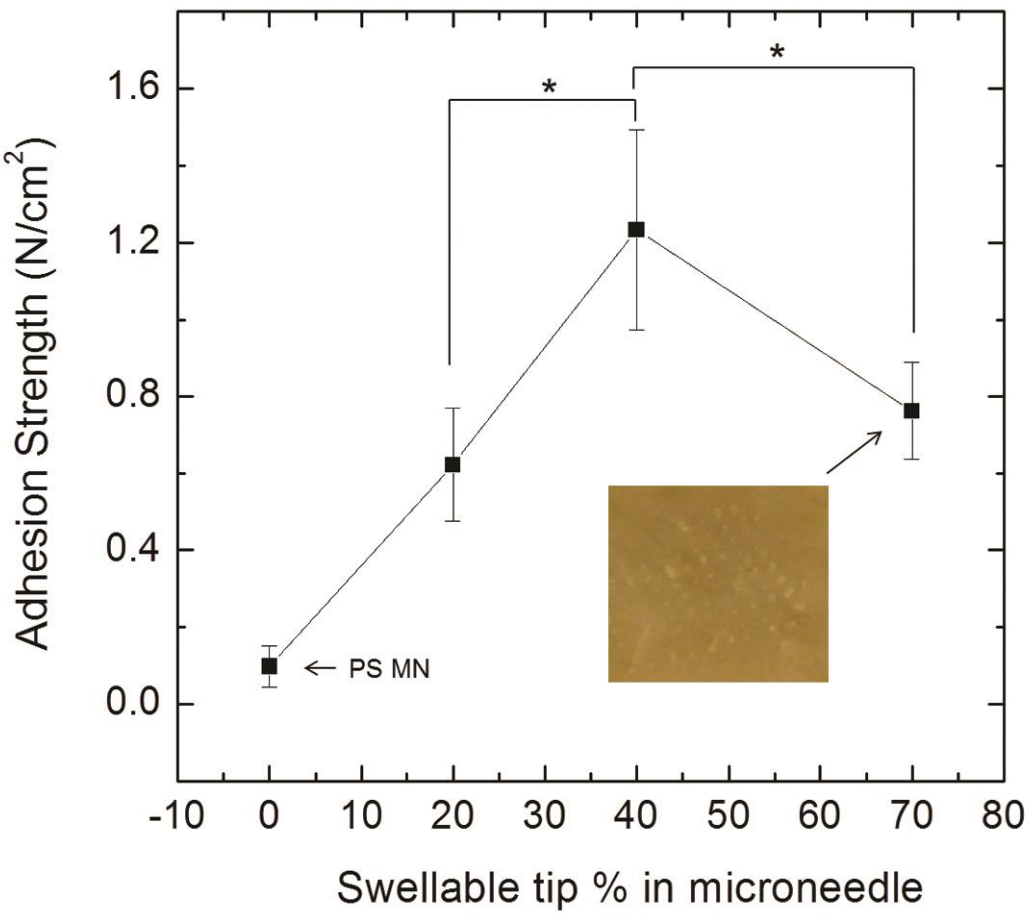

Supplementary Figure S9. Effect of a swellable tip height in the BCP microneedle adhesive on adhesion strength to pig skin. Test samples were applied to the skins with 10 N of preload at 100 mm/min, and held in position for 10 min. Samples were displaced at a rate of 1 mm/min and the force was recorded. The asterisk indicates statistical significance with $p < 0.05$ (one-way ANOVA with post-hoc Tukey's method for multiple comparisons, n=6). In the case of BCP MN with a swellable tip height of 70%, the swollen BCP tips delaminated during pull-out. Error bars represent standard deviation.

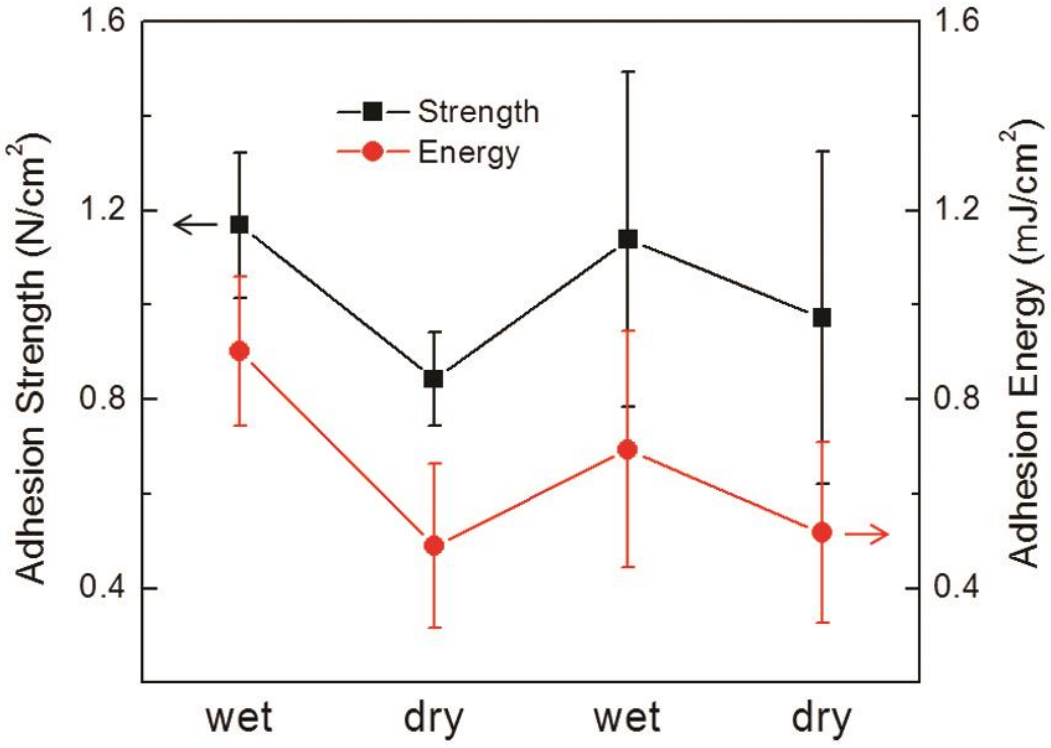

Supplementary Figure S10. Double-layered BCP MN adhesives can withstand multiple cycles of adhesion tests into semi-dry and wet substrates. Dry surfaces were prepared by drying porcine skin on blotting paper until 10~20% of absorbed water was removed. Wet surfaces were prepared by addition of 200μl of water dropped onto porcine skin. BCP MN adhesives were inserted sequentially into wet and dry substrates and were dried at 90^{o}C for 1hr between each insertion. Error bars represent standard deviation (n=4).

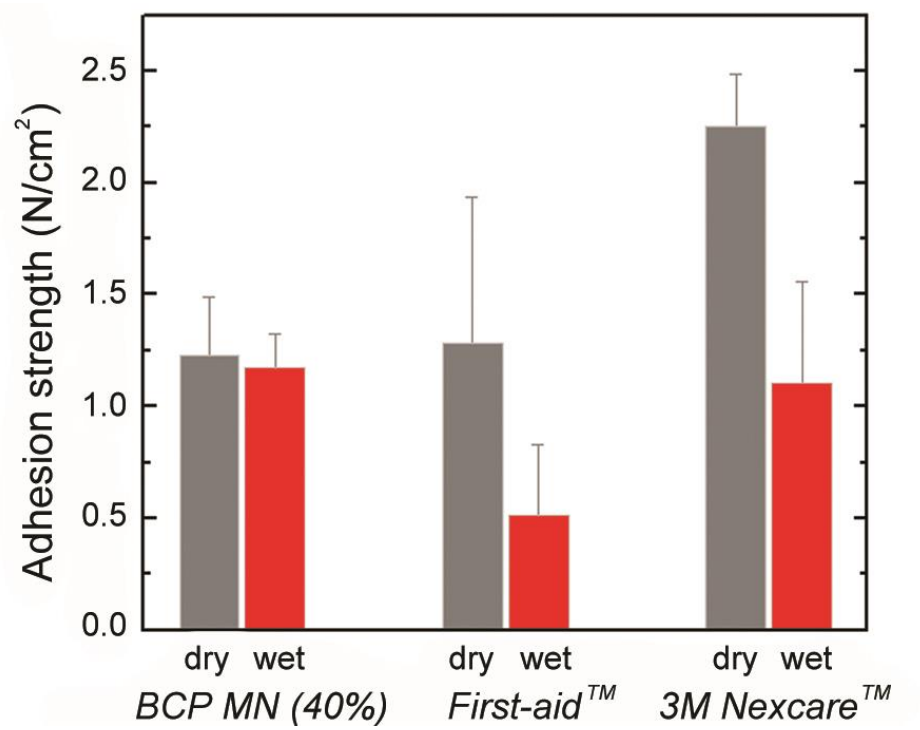

Supplementary Figure S11. Comparison of adhesion with commercial bandages on dry and wet surfaces of pig skin. Wet surfaces were prepared by addition of 200 μl of water on the skin surface prior to application of the adhesives. To measure the adhesion strength of commercial bandages (First-aid™ and 3M Nexcare™), the adhesive part of the bandage was cut into 1 cm x 1 cm patches and bonded with double-sided tape on a flat PS sample. For the duration of all experiments, the tissue was kept moist with PBS. The mean adhesion force was measured from n=5 different samples. Error bars represent standard deviation (n=5).

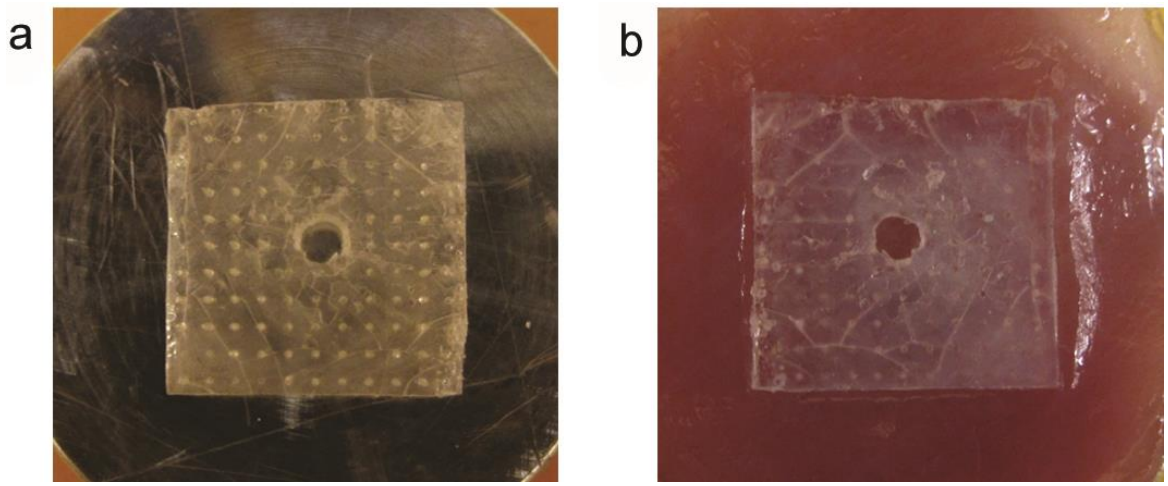

Supplementary Figure S12. Drainage holes can easily be included in the MN adhesive patch. a, BCP MN adhesive with a 2 mm hole designed to prevent accumulation of body fluid at the wound area. b, Photograph after applying BCP MN adhesive with hole onto muscle tissue.

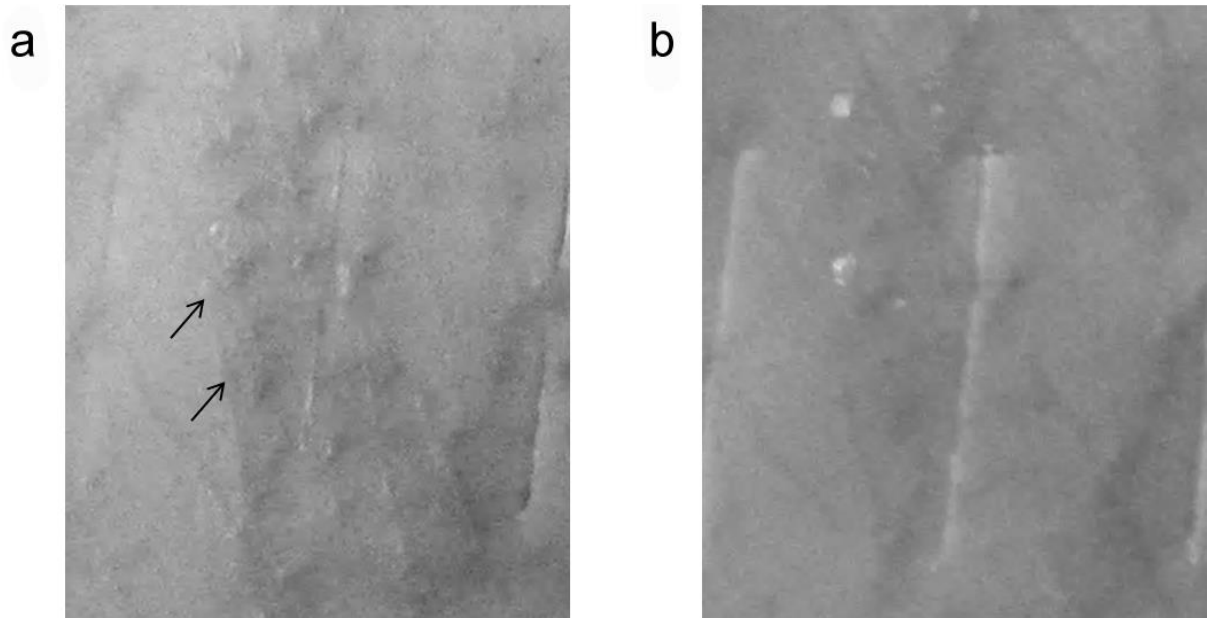

Supplementary Figure S13. Photographs of the pig skin showing puncture marks (arrows in Fig. S13a) following removal of BCP MN adhesive (a) after 0 min and their disappearance (b) after 1 hr. Scratch marks were visible following hair removal via shaving.

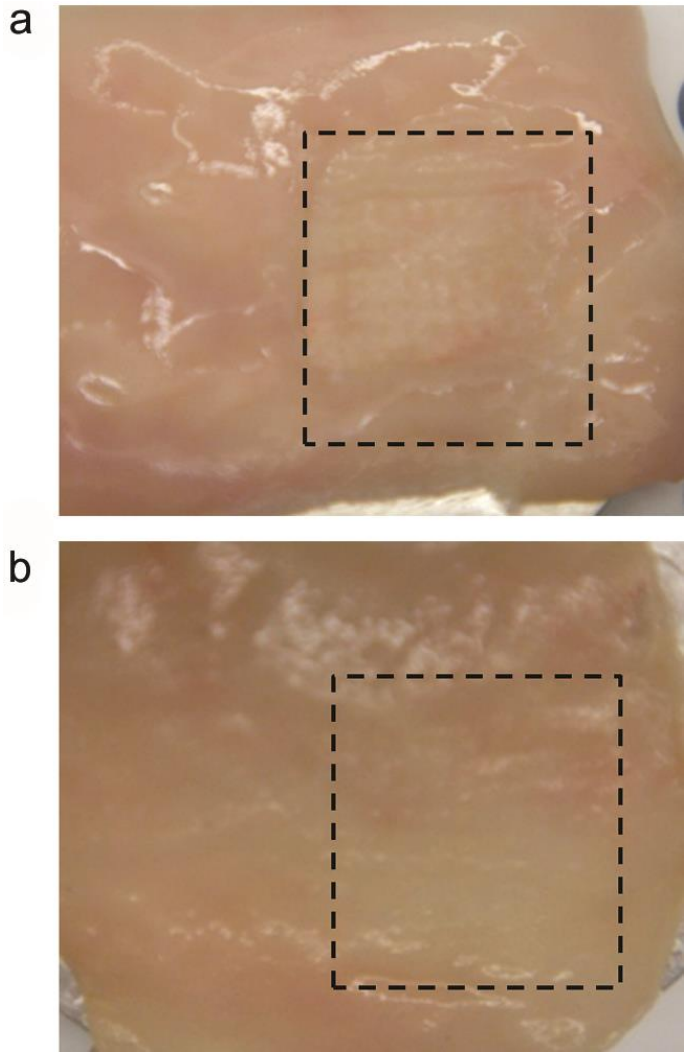

Supplementary Figure S14. Photographs of the serosal surface of intestine tissue showing relaxation and 'resealing' of the tissue at (a) 0 min and (b) 2 hr after removal of BCP MN adhesive. Puncture marks in the tissue disappeared within 2 hr after removal of BCP MN adhesive.

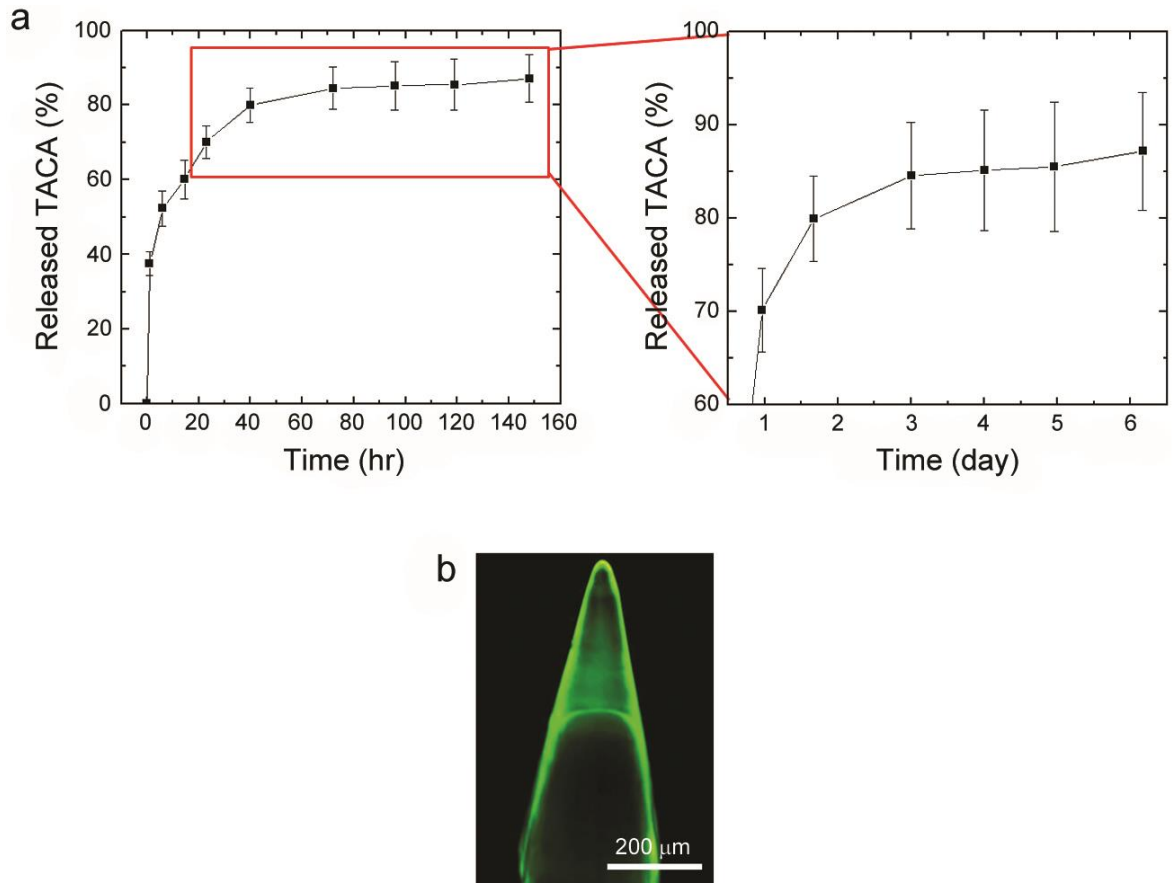

Supplementary Figure S15. a, Release profile of encapsulated triamcinolone acetonide (TACA) from a BCP MN adhesive (10x10 array in 1 cm^2) after direct loading via swelling in a drug solution of 1 mg/ml for 30 mins. TACA continued to release for 6 days. b, FITC-labeled dextran (FITC-dex, M_w: 2,000,000, Sigma) loaded BCP MN. FITC-dex was encapsulated via swelling in FITC-dex solution (4ml) of 1 mg/ml and then BCP MN was visualized via fluorescent microscopy followed by drying at 25^oC for 1hr.

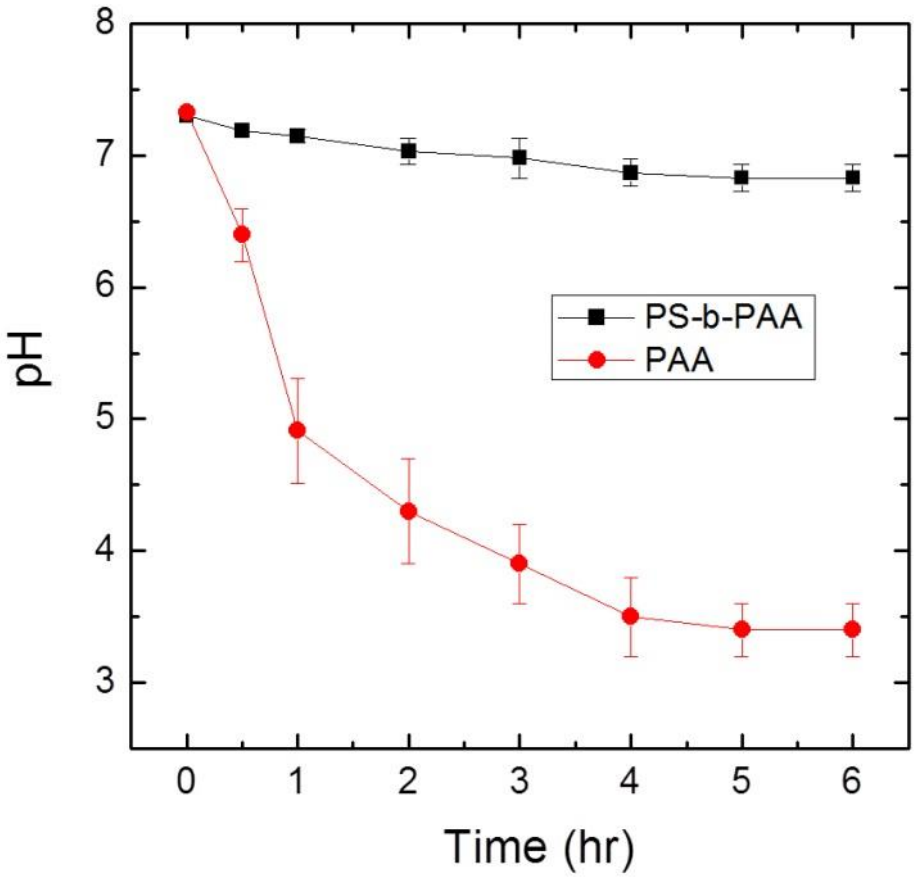

Supplementary Figure S16. pH change of PBS buffer during swelling of PS-*b*-PAA (-■-) and PAA homopolymer (-●-). PAA homopolymer (Mv: 450,000, Aldrich) and PS-*b*-PAA were molded at 180^{o}C. The size of molded specimens was 2 x 5 mm with ~ 1mm thickness. After cooling at room temperature, the specimens were immersed in saline at room temperature and then the pH of each sample was measured at each time point.